Role of π-Radicals in the Spin Connectivity of Clusters and Networks of Tb Double-Decker Single Molecule Magnets

Anis Amokrane, Svetlana Klyatskaya, Mauro Boero, Mario Ruben, Jean-Pierre Bucher

The role of pi-radicals in the spin connectivity of clusters and networks of Tb double-decker single molecule magnets

*Anis Amokrane,[1,†] Svetlana Klyatskaya,[2] Mauro Boero,[1] Mario Ruben,[2] and Jean-Pierre Bucher[1]**

[1]Université de Strasbourg, CNRS, IPCMS UMR 7504, F-67034 Strasbourg, France; [2]Karlsruher Institut für Technologie, Institut für Nanotechnologie, D-76344 Eggenstein-Leopoldshafen

KEYWORDS: Interconnected spin network, π-radicals, single molecule magnets, Kondo effect, Clusters of SMMs, scanning tunneling microscopy, qubit entanglement.

ABSTRACT: When single molecule magnets (SMMs) self-assemble into 2D networks on a surface they interact via the π-electrons of their ligands. This interaction is relevant to the quantum entanglement between molecular qubits, a key issue in quantum computing. Here we examine the role played by the unpaired radical electron in the upper ligand of Tb double-decker SMMs by comparing the spectroscopic features of isolated and 2D assembled entities on surfaces. High resolution STM spectroscopy is used to evidence experimentally the Kondo resonance of the unpaired radical spins in clusters and islands and its quenching due to up-

pairing at orbital overlaps. The presence or the absence of the Kondo feature in the dI/dV maps turns out to be a good measure of the lateral interaction between molecules in 2D-networks. The π-orbital lobes in the 2D network that are linked through the orbital overlap show paired-up electron wave function (one SOMO with spin-up and the other with spin-down) and therefore do not experience the Kondo resonance in the experiment. As a result, small clusters built by STM-assisted manipulation of molecules, show alternating Kondo features of quantum mechanical origin, from the monomer to the dimer and the trimer. On the other hand, the zigzag reorientation observed for $TbPc_2$ molecules in 2D networks is tentatively explained by the repulsive interaction between overlapping SOMO orbitals.

Single molecule magnets (SMMs), made of metal ions stabilized by appropriate ligands, participate in promising strategies of encoding information in single, all identical, units.[1] The mononuclear Bis(phthalocyaninato) Lanthanide (III) complexes ($LnPc_2$) have attracted a great deal of interest,[2] and among them the $TbPc_2$ double-decker has been the most investigated mononuclear SMM in recent years. This success is due to its high magnetic anisotropy barrier and slow relaxation time of the magnetization[3,4] but also to its robustness and evaporability.[5,6] The growth and self-assembly of these $LnPc_2$ double-deckers on surfaces has therefore been addressed by many authors as this represents a prerequisite for their in-depth study by local techniques such as scanning tunneling microscopy (STM).[6-22]

The neutral $[TbPc_2]^0$ complex contains two electronic spin systems: a central $J = 6$ high-spin ($S = 3$ and $L = 3$) with an intrinsic anisotropy arising from the Tb^{3+} 4f-electrons and a S=1/2 π-

radical due to a singly occupied HOMO that is delocalized over the two Pc ligands. Charge and spin state of the $TbPc_2$ molecules may be altered upon adsorption on surfaces.[7–10] A special case is embodied by the monolayer of $TbPc_2$ molecules adsorbed on Au(111) where the π-radical electron survives the adsorption and populates the upper Pc ligand, leading to the experimental observation of a Kondo resonance in the *dI*/*dV* spectra above some specific points of the network.[6,11,12] The absence of Kondo effect on the ligand when the molecule is residing on Cu(111) or Co substrate is rationalized by the fact that the electron in the π-orbital pairs-up with an electron transferred from the substrate due to the much stronger molecule substrate interaction.[7,8] The molecule then bears a negative charge $[TbPc_2]^-$.

Despite the work that has been accumulated over the last decade, the effects of the environment, on the magnetic properties of SMMs is not well understood. In particular, a large impact of the crystalline environment on their magnetic properties has been emphasized.[14,15] If these types of molecules are to be used in future spintronics devices, a better understanding of this phenomenon is compulsory. In the present work, special attention is given to the role played by the radical electrons in the coupling of adjacent SMMs in self-assembled 2D islands or in clusters obtained by STM-assisted molecular manipulation on surfaces. For this purpose, low-temperature (4.6 K), high-resolution scanning tunneling spectroscopy (STS) is used to explore the Kondo resonance of the unpaired radical spins and their quenching due to up-pairing at orbital overlaps. The special status of the π-electrons measured by STS above the ligands of $TbPc_2$ on Au(111)[11,12] and the easy detection of their geometry makes it an interesting system for this study. In particular, due to the weak interaction with the substrate, no f-electrons are involved in the Kondo effect contrary to the case of $DyPc_2$ complexes on Cu(100).[16]

The Tb^{3+} ion with an electronic spin $S = 3$ and an orbital momentum $L = 3$, yields a total electronic angular momentum $J = 6$. Due to the strong spin-orbit coupling and Pc ligand field, the electronic ground state doublet $J_z = \pm 6$ is isolated from the excited state by a gap of several 100 K.[17] The strong magnetic coupling of the Tb^{3+} electron-spin and the radical-spin is ascertained from conductance measurements in supramolecular spin-valve and spin-transistor structures[18,19] where the radical is used as a read-out quantum dot. A ferromagnetic exchange interaction of about 300 mT was measured between the magnetic moment carried by the Tb^{3+} ion and the radical spin ½.[20] In the later set-up, it is the detection of the electronic magnetic moment of the $TbPc_2$ SMM that allows the electronic read-out of the terbium nuclear spin state, with $I = 3/2$ through the hyperfine coupling. A recent RF assisted STS experiment performed at the site of the Pc ligands also yields similar conclusions.[21] As a result, it was suggested that the coupling between the nuclear spin and the radical through the Tb electronic moment could be exploited in quantum information processing (for example by using EPR-NMR sequences) to entangle the spins systems.[20]

RESULTS AND DISCUSSION

The isolated Tb double-deckers on Au(111). The presence of the two Pc ligands promotes face-on adsorption of the molecules on metal surfaces, thus facilitating the investigation of electronic and magnetic properties by high resolution STM/STS. Compact, islands of molecules are easily formed by on surface self-assembly at room temperature.[6,11] However, before we study the monolayer islands of SMM, the local electronic properties of single, isolated molecules on the bare surface must be addressed. For this purpose, single molecules are extracted from a

monolayer island by tip manipulation. The molecule is dragged away from a monolayer island and examined at a distance from it, as is shown in Figure 1a.

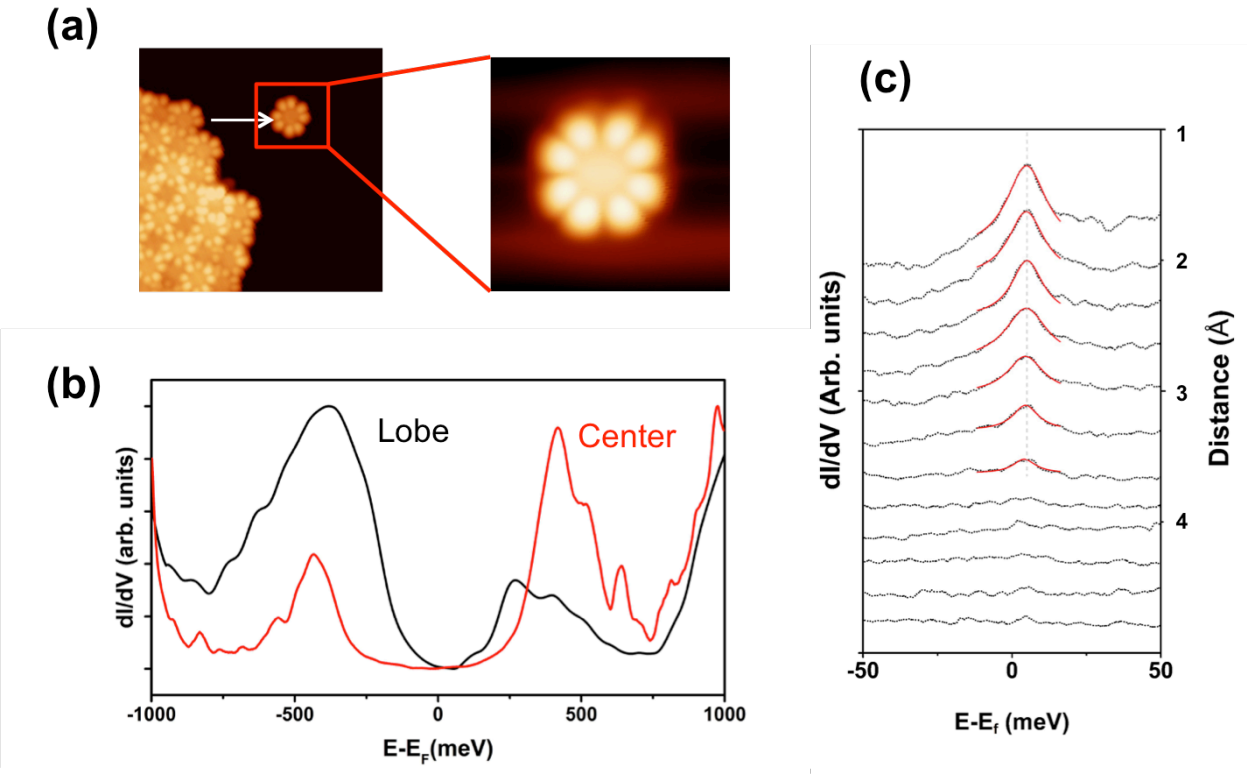

Figure 1. (a) STM images I = 60 pA and V = -0.3 V showing the manipulation of $TbPc_2$ with the tip of the STM (b) STS above the center and a lobe of a single $TbPc_2$ molecule adsorbed on Au(111) substrate with a modulation voltage of 10 mV (rms). (c) By decreasing the modulation voltage to 1 mV (rms) it is possible to evidence the zero bias peak shown here as a function of distance from the substrate.

Figure 1b shows the *dI/dV* spectra recorded above one lobe and above the center of the single molecule at T = 4.5 K. The tip sample distance was stabilized on a free area of Au (111) before opening the feedback loop. Both show a resonance at -0.45 eV which is broader on the lobe while an empty state resonance is found at +0.25 eV above the lobe and +0.40 eV above the center. These resonances are also found in assemblies of molecules and will be discussed later

on, they should not be confused with the HOMO and LUMO (- 0.9 and 0.8 eV) identified in earlier studies of such molecules assembled in domains.[12] Decreasing the modulation voltage amplitude and taking the *dI*/*dV* spectra over an interval between -50 meV to +50 meV above a lobe of the single molecule leads to the spectra shown in Figure 1c. Identical zero bias peaks (ZBP) in the high-resolution *dI*/*dV* spectra are measured above all the eight lobes of the terbium double-decker molecule (see Figure S1). The peak intensity versus tip-sample distance shows a significant decrease in the range from 2 Å to 4.7 Å where it is reduced to the noise level (see Figure 1c). This resonance appears only on the lobes of the upper ligand and vanishes rapidly when the tip is moved towards the center of the molecule. The shape of the ZBP observed on the isolated molecule (Figure 1c) is similar to previously reported Kondo resonances measured above magnetic mono- and double-decker complexes[6, 23-25] which are well described by a Fano function:[26]

$$\frac{dI(V)}{dV} \propto \frac{(\varepsilon+q)^2}{\varepsilon^2+1} \quad \text{with} \quad \varepsilon = \frac{eV-E_0}{\Gamma}$$

where Γ is the width of the resonance, E_0 the peak position and q is the ratio of tunneling into the resonance and into the continuum. The fitting of our data leads to the following values: E_0 = 5.2 meV ± 0.1 meV, q = 3.93 and G = 9.56 meV. Accounting for thermal and modulation voltage broadening[27] on G this leads to a Kondo temperature of T_k = 38 K ± 1 K. Contrary to most transition metal phthalocyanines (TMPc) on metal surfaces, where the Kondo resonance is due to 2D surface-electron scattering by the magnetic atom, here it is the unpaired spin of the π-radicals of the Pc ligand that is responsible for the scattering. The lower Kondo temperature compared with the one of TMPc around $T_K \approx$ 200 K,[24,25,28,29] along with a higher value of the Fano parameter q indicates smaller ligand hybridization to the substrate. Furthermore, moving the

molecule to different places by atomic manipulation leads to the conclusion that the ZBP of $TbPc_2$ on Au(111) is not site dependent nor does it depend on the bottom ligand orientation with respect to crystal directions of Au (111) (see Figure S2). This is quite different from other TMPc systems where the nature of the Kondo resonance might change dramatically as a function of adsorption site.[24, 25]

Molecular clusters by STM based manipulation. In order to understand the evolution of the spin connectivity, from the single object to the molecular film, step-by-step assembling of clusters by molecular manipulation with the STM tip was performed. The attractive potential between the tip and the SMM is used to manipulate laterally the molecule by the so-called pulling procedure.[30] When the tip is moved at a constant height along a predefined path above the surface (feedback loop open), the molecule is dragged on the surface by the tip. If during manipulation, the tip trajectory passes off-center, a rotation of the molecule occurs simultaneously with the translation movement. For the purpose of island construction, both, rotation and translation are used to assemble molecules in their close-packed configuration. While manipulation is a powerful tool, it must be emphasized that appropriate tunneling conditions such as a low current and negative bias voltages are necessary to prevent the molecules from being dragged around by the tip during the scanning process.

Molecular clusters are built step-by-step as described in Figure 2. At each step, the new structure is analyzed by means of *dI/dV* spectroscopy. In the following, the red contour of each molecule represents the molecular orbital extension taken from the isolated molecule (Figure 1). Inside each molecule, a model of the upper Pc is drawn in order to visualize the molecular orientation.

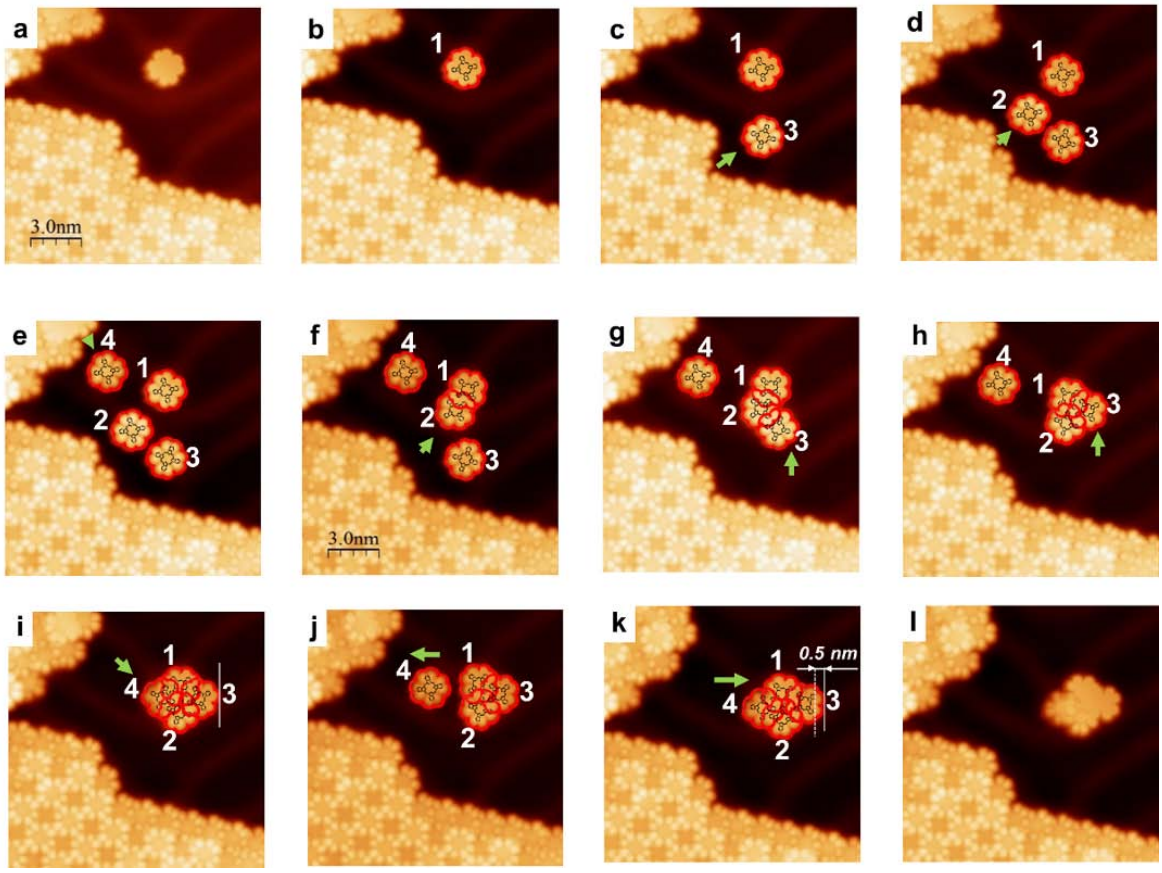

Figure 2. Molecular-manipulation. The electronic distribution of the upper ligand is highlighted in red in order to facilitate the molecular identification during manipulation. (a) and (b) Molecule number 1 is used as a reference. (c) to (e) Molecules labeled 1, 2, 3 are pulled out of the domain as indicated by the green arrows. (f) Molecule 2 is moved towards molecule 1 to form a dimer. (g) Molecule 3 is added to the dimer to form a trimer. (h) Further manipulation on molecule 3 to form a compact trimer. (i) Molecule 4 is inserted into the trimer. (j) and (k) represent the extraction and subsequent insertion with a rotation of molecule 4. After this process, the whole island is translated by 0.5 nm as depicted in (k). (l) Shows the same domain as in (k) without the superposed phthalocyanine model. The tunneling parameters for the topography are I = 70 pA, V = -0.3 V.

Prior to molecular assembly, four molecules have been extracted one-by-one from a large self-assembled domain, as depicted in Figures 2a to 2e. It has been verified that all the isolated molecules exhibit the Kondo resonance on each of their eight lobes. The dimer, trimer, and tetramer are then built by STM manipulation. The process of manipulation is further explained in the Method section. The molecules are moved along a well-defined path until they have reached the optimal molecule-molecule interaction with another molecule on the surface. As an example, the molecule labeled 2 is moved towards molecule labeled 1 to form a dimer as shown in Figure 2f. After manipulation, the molecules in the dimer are oriented parallel to each other, a configuration that does not appear in extended domains (vide infra). The center-to-center distance between the two molecules is 1.45 nm and makes this dimer configuration particularly stable. Spectroscopic measurements performed above the two molecules do not show any ZBP, which indicates an absence of a Kondo resonance on the dimer.

As shown in Figure 2g, when a third molecule labeled 3 is added to the dimer, molecule 2 spontaneously rotates by 6° to adapt to the presence of both, molecule 1 and 3. Again, no Kondo resonance was observed on this molecular chain. In Figure 2h, molecule 3 is further manipulated so as to form a compact trimer. Again, molecules 1 and 2 adapt their orientation to optimize their interaction with molecule 3. As a result, molecule 1 & 3 form a parallel configuration while 1 & 2 and 2 & 3 are staggered with respect to each other. Interestingly, this compact trimer exhibits a Kondo resonance above the intersection of all three molecules with $T_K = 34$ K. No Kondo peak is observed on the other molecular lobes and on the center of the molecule suggesting that this resonance is created by the interaction of all three molecules.

Next manipulation consists in the formation of a tetramer as depicted in Figure 2i where molecule 4 was moved towards the trimer. It is noteworthy that the insertion of the last molecule

does not create any geometrical modification (rotation or translation) of the preexisting trimer. The resulting tetramer island of Figure 2i does not form a square planar geometry and as such cannot be considered as a fragment of the network (see Figure 5b). It may thus be a result of either a minimum energy configuration or a relative minimum whose origin is the sequential island construction by manipulation. To verify this assertion, molecule 4 was extracted from the tetramer (Figure 2j) and subsequently reinserted with a counter-clockwise rotation of 25°, achieving a better match with the former trimer. Pulling harder on molecule number 4 with the STM tip towards the left-hand side produces a displacement of the whole tetramer by 0.5 nm as shown in Figure 2k. This demonstrates the robustness of the tetramer cluster since pulling on molecule number 4 produces the displacement of the entire cluster with no visible fragmentation and ascertains the idea that the molecule-molecule interaction overcomes the molecule-substrate interaction. In the following, the newly formed $TbPc_2$ tetramer is therefore considered as the most stable structure on Au(111). A Kondo resonance with T_K = 31 K is measured on the tetramer of Figure 2k at the overlap of three lobes. No Kondo resonance is found elsewhere on the cluster.

The lobe matching of the different molecular clusters is summarized in Figure 3. When a dimer is formed, the molecular orbitals of the two ligands strongly overlap i.e. two lobes of the first molecule overlap with the same two lobes of the second molecule as is shown schematically in Figure 3a. It is found that interactions between molecules in a cluster are such that only two types of molecular building blocks are found corresponding to the parallel and staggered dimer of Figure 3a. The molecule centers are separated from each other by 1.45 nm in the parallel and 1.62 nm in the staggered configuration respectively. This is very different from the self-assembled domains (see next section) were only single-lobe overlaps are observed between

neighboring molecule. As a result, in the dimer a pairing-up of the delocalized electrons leads to a Kondo quenching everywhere above the dimer.

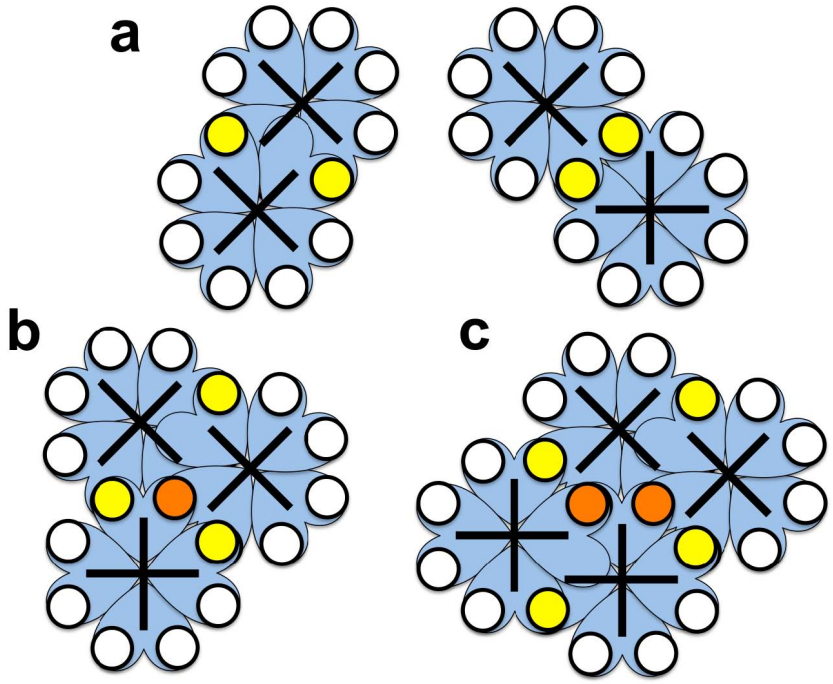

Figure 3. Schematics representation of lobe matching for (a) the parallel- and staggered-dimer, (b) the trimer and (c) the tetramer as observed experimentally. Yellow stands for the two-lobe overlaps (no Kondo) while red stands for three-lobe overlap showing an experimental Kondo feature. The white circles do not show measurable Kondo signal.

In the compact trimer, the only spot that shows a Kondo resonance is the one consisting in three overlapping lobes in the center of the cluster as shown in the schematics of Figure 3b by the red spots. This comes about because the three single electron wave functions overlap at this point yielding a net spin. It is noteworthy that not more than three lobes are allowed to overlap at the same time in a molecular cluster. Therefore, larger 2D clusters can always be regarded as fragments of trimers. Similar to the case of the large self-assembled domains, no Kondo

resonance is observed on the lobes at the perimeter of the clusters. The relaxation of the outer lobes probably yields a too low Kondo temperature to be measured experimentally.

When an isolated molecule is dragged towards an already formed 2D cluster the molecule snaps-in to the available space at the perimeter of the cluster, simultaneously adjusting its azimuthal angle. The tetramer is thus formed from the trimer in a well-defined manner as shown schematically in Figure 3c. It involves the same type of orbital overlaps as the trimer (two red spots in Figure 3c) and therefore shows a similar Kondo temperature, i.e. $T_K = 31$ K.

Table I summarizes our measurements in terms of geometry related Kondo temperatures. As will be shown in the next section, the geometrical arrangement of $TbPc_2$ molecules in self-assembled domains (anticipated in Table 1) are different from those observed in small clusters. One may wonder at which stage the small cluster structure switches to the 2D semi-infinite structure.

Table 1. Molecular clusters, specific locations of Kondo resonance, Kondo temperatures measured at specific locations and STM images for each entity of Tb double decker SMM on the Au(111) substrate.

Cluster	Kondo resonance	T_K (K)	STM image
Monomer	On all 8 lobes	38	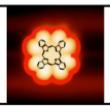
Dimer	No Kondo	N/A	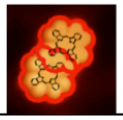
Trimer (chain)	No Kondo	N/A	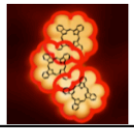
Trimer (compact)	On 3-lobe overlap	34	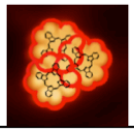
Tetramer (compact)	On 3-lobe overlap (2 places)	31	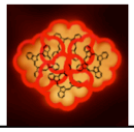
Domain	On non-overlapping lobes	22	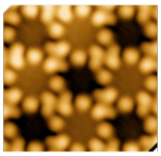

A theoretical analysis is necessary to obtain a better understanding of the elementary processes that are at the origin of orbital overlap and Kondo behavior when the clusters are formed. Unfortunately, first-principles calculations involving several molecules of rare earth complexes in contact with a metal surface are hardly tractable. Therefore, in our approach a DFT calculation is performed to estimate the variation of the electronic structure when a dimer is formed in the absence of any substrate. We first calculated the electronic structure of the monomer. The gap between the highest occupied and the lowest unoccupied level is E_g(mono) = 640 meV and compares well with the experimental value of 760 meV. As expected, the highest occupied level is a SOMO, that is a singly occupied molecular orbital. More information on the monomer can be found in Figure S3. Second, for the dimer calculation we consider the two geometries

observed experimentally: (1) the parallel (//), and (2) the staggered (⊥) configurations (Figure 3a). The molecule centers are separated from each other by 1.45 nm in the parallel and 1.62 nm in the staggered configuration respectively. In the parallel configuration one molecule is shifted 1.34 nm parallel and 0.59 nm perpendicular with respect to the first one.

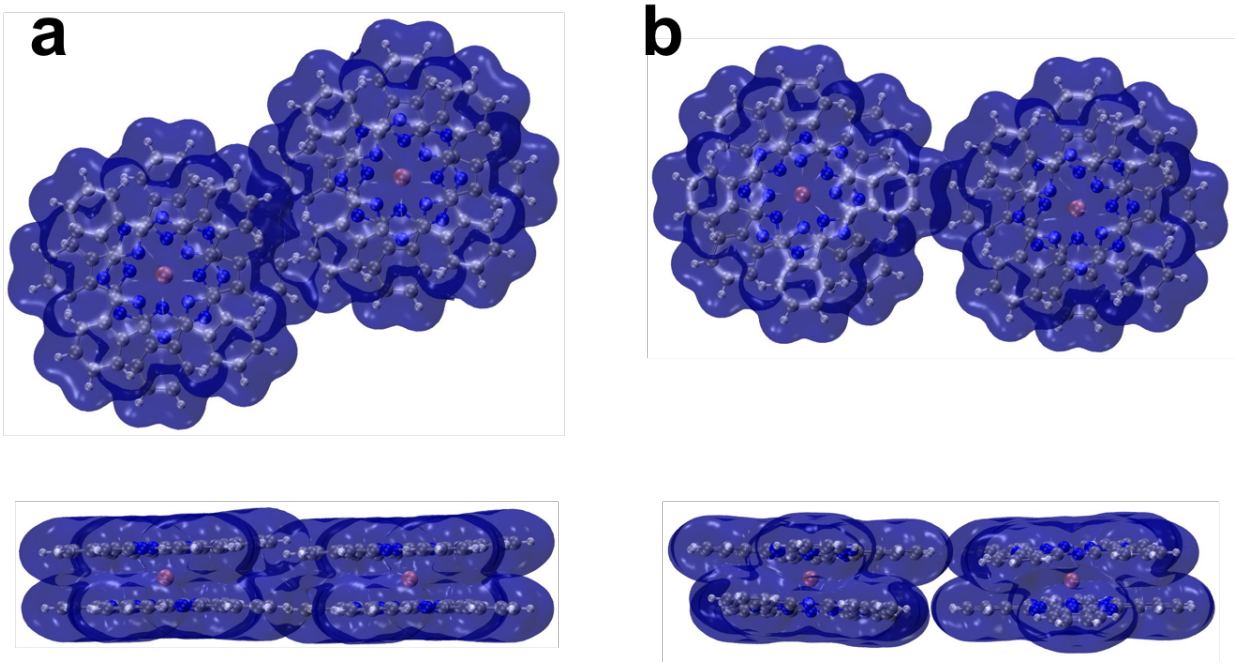

Figure 4. DFT calculation of the electronic density distribution at a value of 0.001 e/Å^3 for two dimer configurations, top- and side-view respectively. (a) Parallel-configuration: the Tb-Tb distance is $d(//)$ = 14.48 Å. (b) Staggered-configuration: the Tb-Tb distance is $d(\perp)$ = 16.20 Å. The color code for atoms is H: White, C: Grey, N: Blue, Tb: Red.

The calculated electronic density distributions of Figure 4 show that in both cases, the molecules fit perfectly, one into the other with the usual structure in which the top and the bottom Pc ligands are rotated by 45° with respect to each other. The nesting however is more efficient in the parallel configuration which is reflected in the fact that the parallel configuration is lower in energy by 300 meV and therefore constitutes the ground state. This is also by far the

most frequent structure observed experimentally for isolated dimers; the staggered structure only appears as a part of larger clusters. The energy gap between the occupied and the unoccupied levels is $E_g(//)$ = 260 meV and $E_g(\perp)$ = 120 meV for the parallel and the staggered geometry respectively. The stability of the parallel configuration compared to the staggered one is also reflected in its larger energy gap. Interestingly, the total wave function of the system in both configurations corresponds now to a singlet HOMO, i.e. paired up electrons. This is in good agreement with the experiment that shows a quenching of the Kondo resonance upon the dimer formation. Figure 4 clearly shows the interpenetration of the electronic density distribution for both geometries, in accordance with the STM images of Figure 2 and the models of Figure 3. Furthermore, a close examination of the HOMO over the dimer in Figure S4 shows, as expected, the phase continuity of the wave function at the intersection (same color means same phase). These calculations are very demanding and cannot be continued on larger clusters for the moment, however we believe that they convincingly shows the main trend which is stability, SOMO paring-up and the gap structure.

Self-assembled monolayers of Tb double-deckers on Au (111). In the following the same approach is applied to the analysis of molecules assembled in a network. When the $TbPc_2$ molecules are adsorbed on Au(111) at 300 K they tend to form islands of various sizes as depicted in the STM image of Figure 5a. As first pointed out by Komeda et al.[11] the STM image of the self-assembled monolayer reveals a checkerboard contrast of molecules (see Figure 5b). Bright and dark molecules (marked A and B respectively) correspond to $TbPc_2$ molecules in two different states. A closer examination of the STM images reveals that upon condensation of the 2D phase from the isolated molecules, each molecule shares 4 of its lobes, out of eight, with

adjacent molecules of the network (along A-B or B-A); the other 4 lobes out of eight (along A-A or B-B) do not overlap. The even distribution of overlapping lobes on the perimeter of the molecule is induced by the symmetry of the semi-infinite lattice and clearly distinguishes the lattice from the clusters. Unit cell vectors of such compact domain are labeled $\boldsymbol{a_1}$ and $\boldsymbol{a_2}$ with the following lattice parameters: $a_1 = a_2 = 2.0 \pm 0.1$ nm. The next neighboring molecules are identified by the vectors $\boldsymbol{b_1}$ and $\boldsymbol{b_2}$ where $b_1 = b_2 = 1.42 \pm 0.05$ nm. The angle is $\alpha = 90° \pm 1°$ in both lattices. The later values are in good agreement with with those that can be extracted from eralier work.[11,13,23]

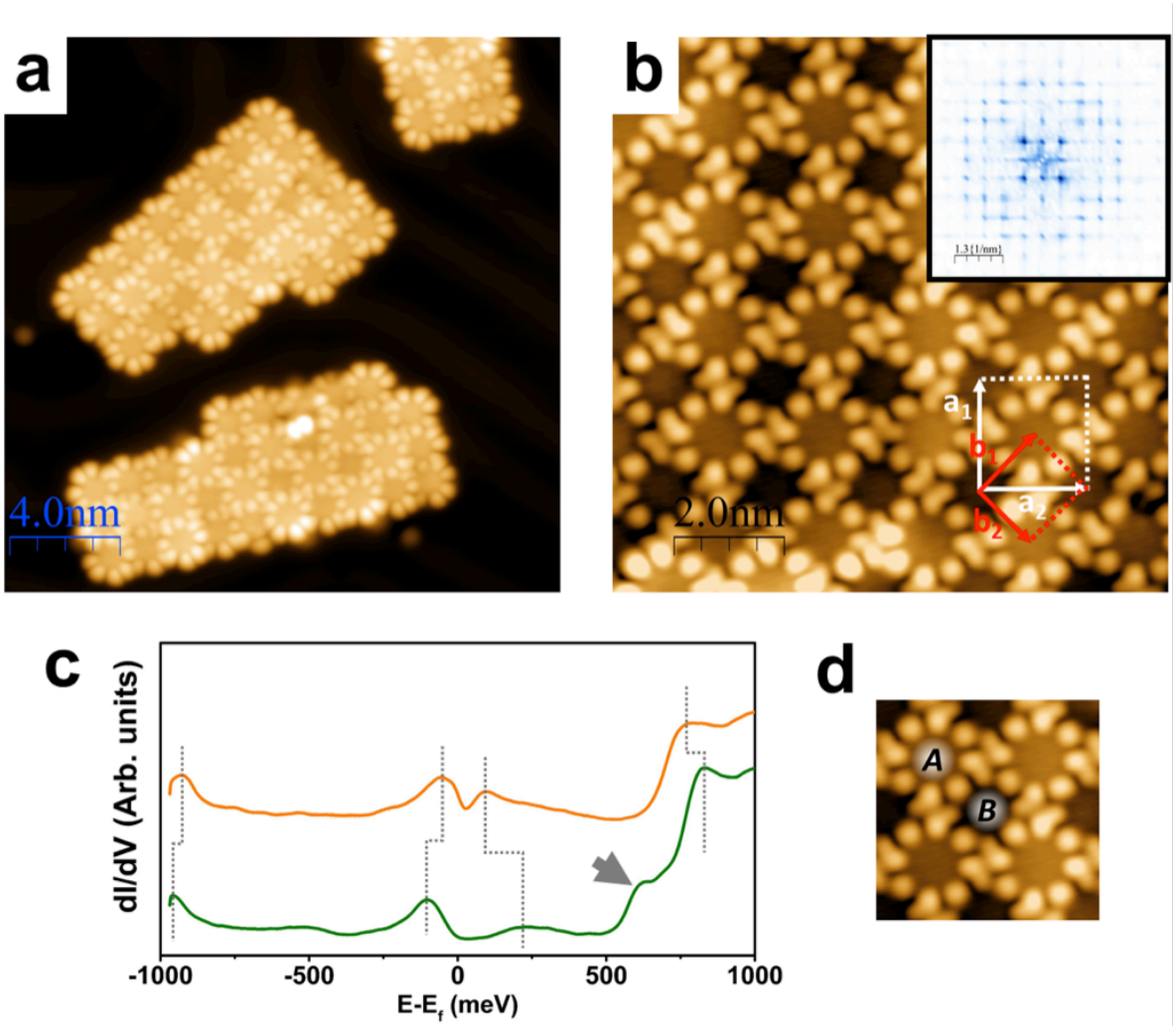

Figure 5. (a) and (b) Constant-current topographies of $TbPc_2$ molecular islands grown on Au (111). Corresponding 2D FFT of the molecular domain is depicted in the inset of the top right corner of (b), the bar corresponds to 1.3 nm^{-1}. Two lattice vectors are highlighted. $\boldsymbol{a_{1,2}}$ represent the lattice parameters of one molecular type, $\boldsymbol{b_{1,2}}$ those of the next neighbors. Two topographic contrasts are observed for molecules in a domain. The bright ones are labeled A and the dark ones are labeled B. (c) *dI*/*dV* spectroscopy performed at the center of both A-type (red) and B-type (black) molecules. Vertical dotted lines show the correspondence between different peaks. A supplementary LUMO peak appears for B-type molecule at 620 meV. (d) Topography image showing the places where spectroscopy was performed.

The spectra recorded above the center of A- and B-type molecules are shown in Figure 5c, they look quite different from those of the isolated molecules (Figure 1b). The two resonances on either side of the Fermi level are now close together. This tendency of gap reduction upon formation of the cluster units was already emphasized on the basis of the calculation for the dimer in the previous section. Since in both cases (isolated and self-assembled) the molecules rest on the same Au(111) substrate, it can only result from the lateral interaction among molecules. The difference of A- and B-type molecules in the STS spectra of Figure 5c is materialized by the vertical dotted lines. The two features at -0.9 eV and +0.8 eV do not shift significantly and are similar to those reported on other metalo-phthalocyanine molecules[12,13,16,22] and sometimes identified as HOMO and LUMO.[12] The two resonances that are closest to E_f are separated by only 150 meV above the A-type molecule and 320 meV above the B-type molecule. Quite remarkable is the additional peak in the unoccupied states observed at +620 meV on the B-type molecule, which may well be the distinguishing mark of the dark (B) compared to the bright (A) molecule after self-assembly.

While the above *dI/dV* measurements demonstrate the presence of two kinds of $TbPc_2$ molecules inside a monolayer, it is hardly sufficient to conclude on the conformation of individual molecules within the network. For this purpose, more sensitive tunneling conditions ($V \approx 10$ meV and $I \approx 10$ pA) were used in this work to visualize the molecular orbitals of the inner part of the molecules. Figure 6a shows a high resolution STM image of a terbium double-decker monolayer on Au(111). The different orbital distribution in the center of A- and B-type $TbPc_2$ molecules are now clearly visible as highlighted in Figures 6b and 6c. The "external lobes" are simultaneously visible but due to contrast enhancement they now appear as large black dots. Notice that inside a given A- or B-molecule, the inner and outer lobes possess the same phase. These results are consistent with the calculated MO distribution obtained by DFT calculation by Vitali & al.[7]

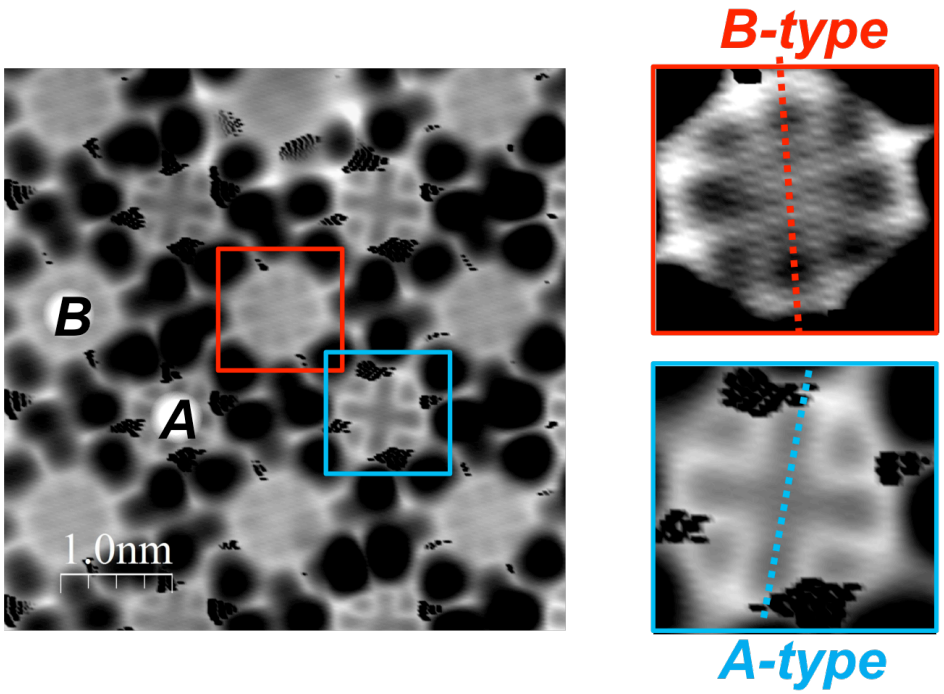

Figure 6. High-resolution constant-current topography, $I = 70$ pA and $V = -50$ mV. Under these conditions, A and B show two different electronic distributions of the central part of the

molecules. Magnified images: B-type molecule show eight distinct spots while A-type molecules show extended "lobes" leading to a cross like contrasts in the center. Two lines are drawn on both images to highlight the different orientation of the inner lobes of A- and B-type molecule.

The angle between the two lines in Figure 6b and 6c represents the smallest angle between lobes and is found to be equal to 15°. This value is in accordance with the work of Komeda *et al*.[11] who first postulated a different orientation of A- and B-type molecules based on the observation of four hardly distinguishable lobes of B-type molecules from conventional topographic images. Ultimately, the results of Figure 6b and 6c not only show a different orientation of A and B-type molecules they also show different contrasts providing information on the relationship between upper and lower Pc ligand (to be analyzed further). It is clear for example that by keeping a 45° azimuthal angle between the upper and the bottom ligands (as in the isolated molecule of Figure 1) a forbidden structural overlap leading to steric repulsions would occur. Therefore the only way to accommodate the bottom ligands is by assuming the same orientation for all of them, similar to monolayer MPc molecules.[31,32] In this case two configurations of the $TbPc_2$ with different azimuthal angle are obtained. The reduction of the apparent height of the B-type molecules by 0.3 Å compared to A-type molecules in the STM topography (see Figure 5d) results from the different azimuthal angle, since the substrate effect is assumed to be similar in both, A- and B-type molecules, due to the negligible upper ligand-substrate interaction. The above results, in accordance with earlier ones,[12] demonstrate that the electronic property of an assembly of molecules can be very different from that of an isolated molecule, as a result of the large influence of inter-molecular interactions. The lateral bond

formation between Co-porphyrin molecules was likely found to change the molecule-substrate separation and thus the Kondo screening of the metal centers.[33]

As a result of the decoupling, an interesting correlation was established by Komeda et al.[12] between the unpaired pi-electron orbital energy and the Kondo resonance in a special situation where some molecules in the monolayer are tilted and consequently show a wide range of energy distribution of the SOMO on all the 8 lobes of the molecule. This effect has been attributed to a changing interaction of the upper ligand with the substrate due to the tilting. We also found similar sharp peaks on specific (defective) molecules, however in the present work we focused on the current situation observed on a large scale in extended domains of molecules where the SOMO is well defined (does not shift). Our measurements then show that the Kondo resonance only appears on one lobe out of two, namely those that do not have an overlap with a neighboring molecule.

In the following we show that the STS measurements provide a deeper insight into the local electronic properties of adsorbed molecules since it ideally allows making links between the spectroscopic features of the condensed 2D phase and those already present in the isolated molecules. Figure 7a shows *dI*/*dV* spectra recorded above the three regions indicated in the topography image of Figure 7b. The spectra acquired above the center of an A-type molecule (red) and above the overlap of two adjacent double-deckers (blue) are similar although the spectrum recorded above the overlap exhibits a larger gap of about 300 meV compared to 150 meV above the center. On the other hand the spectrum acquired above the non-overlapping lobes (green), exhibits an occupied level that is strongly downward shifted to -500 meV while the excited level is upward shifted to +260 meV. As a result, the gap above non-overlapping lobes is 760 meV. It is remarkable that the spectra acquired above non-overlapping lobes, between four

adjacent $TbPc_2$ molecules (Figure 7a upper spectrum) show the same features at -500 meV and at +260 meV as the spectra observed above the lobes of an isolated single molecule in Figure 1b. Furthermore, a careful study by high resolution STS, shows that the non-overlapping lobes are also those leading to the detection of a zero-bias peak (ZBP) related to a Kondo effect (inset of Figure 4a) with $T_K \approx 22$ K. Same measurements above the overlapping lobe (one molecular lobe out of two) do not show any evidence for a Kondo effect. The Fermi-liquid origin of the ZBP at $TbPc_2$ on Au(111) has been ascertained in an experiment realized under similar conditions as a function of temperature and external magnetic field.[11] Our findings furthermore demonstrate a clear correlation between the wide-range spectroscopic features (Figure 7a), and the simultaneous appearance of a Kondo resonance. The reoccurring gap, related to the appearance of the Kondo resonance provides conclusive evidence that the peaks at -500 meV and +250 meV are due to the single electron occupied SOMO and corresponding unoccupied state.

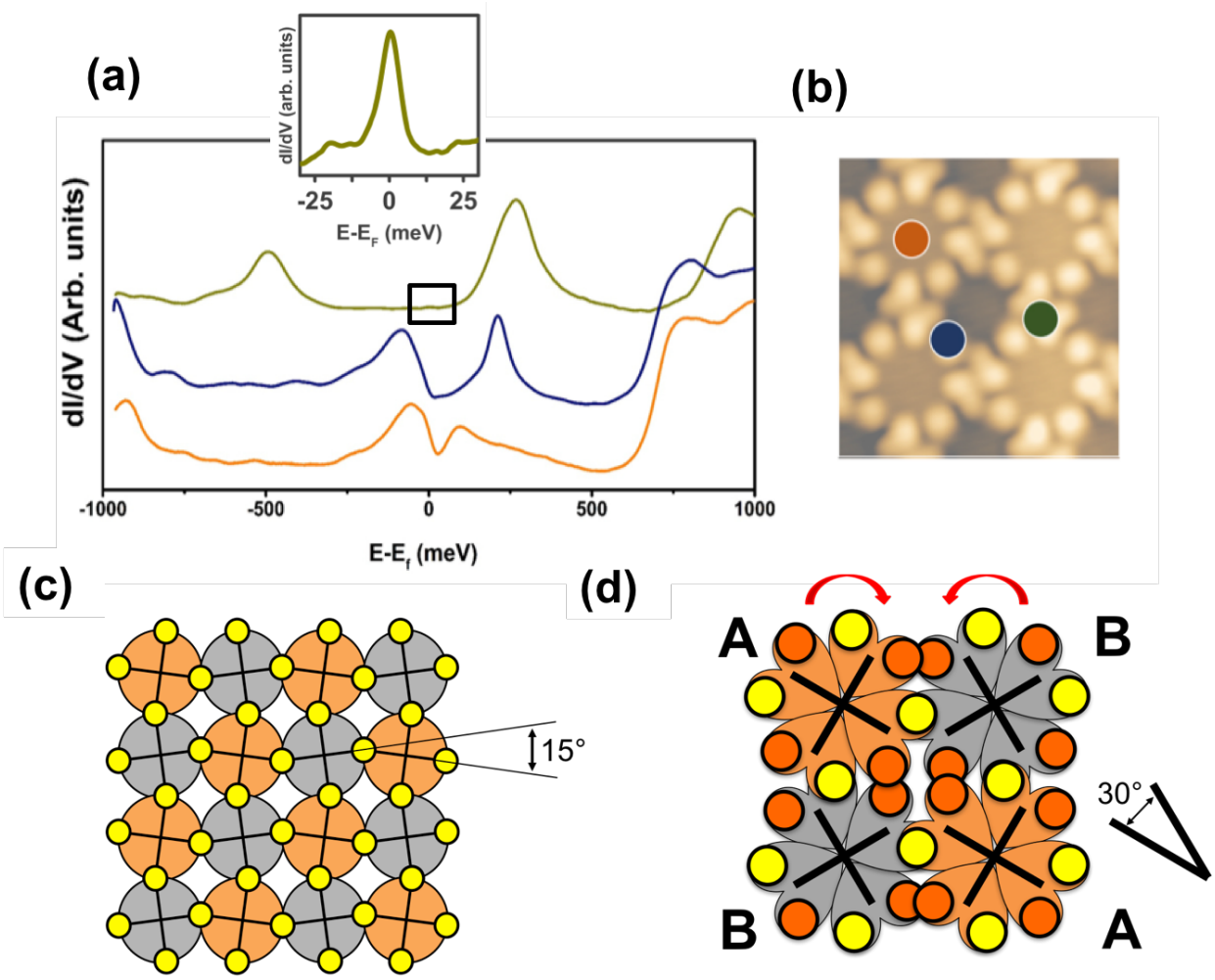

Figure 7. (a) *dI/dV* spectroscopy performed above the three regions as shown in the topography image (b). The inset in (a) shows a close-up of the ZBP spectrum acquired above the non-overlapping lobes between 4 molecules indicated by a green dot in the topography with a lower modulation voltage. (c) Schematics representation of the network formed by the overlapping lobes (yellow) of A- and B-type molecules. (d) Unit cell showing 4 adjacent molecules with the proper orientation inside a network. The bright yellow lobes are as before, common to A- and B-molecules. The red lobes on the contrary are the "dangling" lobes belonging to either A- or B-molecules. The bold cross describes the orientation of each molecule while the red arrows refer to the different chirality of A- and B-molecules.

The Kondo resonance observed above in monolayer networks exhibits a lower Kondo temperature $T_K \approx 22$ K than the isolated $TbPc_2$ molecule on Au (111), for which $T_K \approx 38$ K. Even though the same radical spin is responsible for the Kondo resonance in both cases, this difference refers to a more efficient screening for the isolated molecule. Keeping in mind that only the spin properties of the upper Pc-ligands are accessible by STS, there is much to learn from the spatial distribution of the Kondo signal since it is affected by the presence of the neighboring radicals. Radicals have been investigated extensively in the context of molecular magnetism, in particular the SOMO-SOMO overlap has been recognized to play an important role in the magnetic ordering of crystals made of neutral organic radicals.[34,35] Here we discuss further the reason why the Kondo resonance survives the self-assembly on some parts of the molecular network and is quenched otherwise.

STM-topography images show unusual extension of the molecular orbitals of $TbPc_2$ double-deckers on Au(111) as can be seen from the superposed atomic skeleton in Figure S2, where the orbitals are significantly bulging out of the molecular framework, way beyond the normal atomic positions, in contrast with the single Pc ligand in direct contact with the surface that does not show this effect. Such a large extension of molecular lobes in STM images is typically found for aromatic molecules that are decoupled from the substrate by some ultrathin insulating layer.[36-38] The lobes of such Pc radicals are prone to couple with those of neighboring molecules, because the intermolecular overlaps of such singly occupied molecular orbitals (SOMO) tend to adopt a bonding character. The interpretation of the STM data then becomes straightforward since the lobes in the 2D network that are linked through the orbital overlap show paired-up electron wave function (one SOMO with spin-up and the other with spin-down) and therefore do not experience the Kondo resonance in the experiment. The schematic views in Figure 7c and 7d show the lobes

observed in the STM experiment. Among the 8 lobes of each molecule, 4 of them have an overlap with the neighboring molecules (yellow spots in Figure 7c). For symmetry reasons, the 4 overlapping lobes lie on the 4 branches of a cross. Each B-cross is rotated by 15° with respect to the A-cross which leads to the 2D zigzag network shown in Figure 7c. As shown in Figure 7d, it is the specific bond with the neighboring molecule i.e., every second (yellow) lobe that leads to the reorientation by 30° of B-type molecules with respect to A-type molecules. In fact the overlap and avoided overlap both together, which can be understood in a simple way by noticing the repulsive character of paired-up SOMO lobes, similar to VSEPR model for simple molecules.[39]

On the other hand, our STS measurements show that the 4 unpaired lobes per molecule (orange dots in Figure 7d) still show a Kondo resonance, even though the screening by the substrate electrons is less efficient. An estimate of the interaction between radicals spins S = ½ is obtained from the magnetic characterization of $[YPc_2]^0$ bulk material (no f-electrons) where an antiferromagnetic radical-radical interaction of about 1 K has been measured.[40,41] This value is comparable with the exchange interaction between the radical and the Tb electron spin.[20] A clear picture thus appears, where a network of Tb electronic moments is mutually coupled through the radicals, this network, in turn, provides an efficient screening for the weakly coupled nuclear spin system.

Finally, the coupling of the SMM through the network indicated in Figure 7d induces a new kind of electronic chirality. For symmetry reasons, the overlapping lobes are not the same in A- and B-type molecules, i.e. the overlapping lobe is positioned clockwise in A-type while it is positioned counterclockwise in B-type molecules (see Figure 7d), thus forming racemic domains. Here the electronic nature of the molecule is modified by spin-pairing with the neighboring

molecule, it is different from the chirality induced by the substrate[16] or the one induced by STM tip-manipulation.[9]

The geometrical arrangement of $TbPc_2$ molecules in small clusters are different from those observed in self-assembled domains were only one lobe overlaps with a neighboring molecule. One may now answer the question concerning the point (stage) at which the small cluster structure recovers the 2D semi-infinite structure. At least a sizable number of molecules must have a network environment (4 neighboring molecules) and a number in excess of a few ten molecules are necessary for that, as can be seen in Figure 5a where the checkerboard motif is still perturbed at the edge of small islands. The geometrical and magnetic arrangements of $TbPc_2$ molecules in this work have been explained exclusively by the stability provided by overlapping orbitals to such an extent that it appears like the main driving force in the assembly process. It is however based on arguments that have been developed quite early and used in predicting the geometry of pi-pi interaction.[42]

CONCLUSION

In summary, we have used high-resolution STM-spectroscopy to evidence experimentally the spin networking of SMMs. Our analysis is based on the identification of the MO lobes in the STM images of molecular networks. The Kondo effect was used as a dedicated tool to follow the presence of unpaired radical spins on the orbital lobes of the upper ligand of a $TbPc_2$ SMM. It is found that the double-decker molecules are linked through long-range orbital overlaps leading to a quenching of the Kondo resonance while the lobes that are not involved in the overlaps keep their normal single molecule Kondo features. The magnetic exchange interactions resulting from the overlapping orbitals lead to a fully connected spin network. Furthermore it is found that the

molecular arrangements of small compact clusters built by STM-assisted molecular manipulation, are different from those observed in the extended domains. The symmetry breaking of the finite system (directional interaction) compared to the infinite lattice then leads to more than one orbital overlap between two adjacent molecules. However, the experiment shows that in all cases the structures are made of two types of dimer fragments, parallel and staggered. Our findings open up new ways to detect the lateral interaction among molecules in both, self-assembled as well as tip manipulated molecular assemblies and demonstrate that the Kondo effect is a dedicated tool to follow the spin networking driven by radicals. The "bottom-up" approach adopted here may help in designing and engineering chemically tailored molecules with the desired electronic structure and magnetic behavior.

METHODS

Experimental Details. All sample preparations were carried out in an ultrahigh vacuum (UHV) system with a base pressure of 1 x 10^{-10} mbar. The single crystalline Au(111) substrate was cleaned by Ne^+ sputtering and annealing cycles. The powder of $TbPc_2$ molecules (synthesized by the Ruben group at the Karlsruhe Institute of Technology) was first degassed *in-vacuo*, at a temperature slightly below the sublimation temperature for 24 hours. Deposition of $TbPc_2$ occurred at a sublimation temperature of 600 K onto the Au(111) kept at room temperature. Molecule sublimation was performed in a side chamber of the UHV system; during this operation the pressure was kept below 1 x 10^{-9} mbar. All STM/STS data were acquired at 4.5 K. STS spectra were measured using a lock-in detection with a modulation between 1 mV and 10 mV (rms) depending on the features to be resolved.

Molecular manipulation was carried out by means of the "pulling" procedure i.e. the molecule-tip interaction is used to laterally manipulate the molecules by means of an attractive potential. The tip was positioned 4 Å above the surface before the feedback loop is opened. When the tip is moved at constant height above the surface, the molecule is dragged along a well-defined path on the surface. For the purpose of cluster construction both, molecular rotation and translation were used. The tunneling current is monitored as a function of *x-y* coordinates for a better control of the manipulation process. The building of a molecular cluster is easily performed by separately manipulating single molecule towards a specific area. In this way up to four molecules, forming a tetramer, could be successfully assembled. The manipulation was achieved using a bias voltage $V = 0.1$ V and a current $I = 4$ nA. We considered that the optimal geometry of the cluster was reached when the molecule to be added to the cluster could not be moved further under the same condition. After each manipulation the new structure was investigated by means of dI/dV spectroscopy.

Computational Methods. We resort to first principles simulations within the density functional theory[43] (DFT) framework as implemented in the CPMD[44] code. The Becke exchange[45] and the Lee-Yang-Parr correlation[46] functional have been used to describe the exchange and correlation contributions, complemented by the exact exchange[47] (B3LYP). Core-valence interactions have been described by norm-conserving Troullier-Martins[48] pseudopotentials (PPs) for N, C, and H, while for Tb we make use of a Goedecker-Teter-Hutter[49] semicore PP. Valence electron orbitals were represented in a plane wave (PW) basis set with a cut-off energy of 80 Ry. To eliminated the problem of periodically repeated images, typical of standard PW approaches, an isolated cell[50] with an edge of 47.7 Å was used. A spin-unrestricted approach is adopted in all the simulations and van der Waals interactions were included

according to Grimme's D2 formula.[51] All structures have been fully optimized until residual atomic forces are smaller than 10^{-4} hartree/bohr.

ASSOCIATED CONTENT

Supporting Information. The Supporting Information is available free of charge on the ACS Publication website at DOI: .

Constant current STM images of a single Pc^{-2} molecule and a Tb double-decker molecule on Au(111) imaged with atomic resolution, contrast and extension of molecular lobes. Detailed analysis of adsorption site, molecular conformation and respective orientation of bottom and top ligands on the Au(111) surface (PDF)

AUTHOR INFORMATION

Corresponding Author

*E-mail: jean-pierre.bucher@ipcms.unistra.fr

Present Addresses

† Present address: Department of Physical Science and Engineering, Nagoya University, Japan.

Notes

The authors declare no competing financial interest.

ACKNOWLEDGMENT

JPB thanks the Institut Universitaire de France for financial support. We acknowledge support from EquipEx Union No. ANR-10-EQPX-52 and LabEx NIE: ANR-11-LABX-0058_NIE. M.B.

thanks Pôle HPC and Equipex Equip@Meso at Unistra, and Grand Equipement National de Calcul Intensif (GENCI) under allocation DARI-A2 A0020906092.

REFERENCES

1. Wernsdorfer, W.; Sessoli, R. Quantum phase interference and parity effects in magnetic molecular clusters. *Science*, **1999**, 284, 133.

2. Lan, Y.; Klyatskaya, S.; Ruben, M. Bis(phthalocyaninato) Lanthanide (III) Complexes – from Molecular Magnetism to Spintronic Devices in Lanthanides and Actinides in Molecular Magnetism (p. 223-292), Wiley-VCH Editor.

3. Ishikawa, N.; Sugita, N.; Ishikawa, T.; Koshihara, S.; Kaizu, Y. Lanthanide double-decker complexes functioning as magnets at the single-molecular level. *J. Am. Chem. Soc.* **2003**, 125, 8694.

4. Takamatsu, S.; Ishikawa, T.; Koshihara, S.; Ishikawa, T. Significant increase in the barrier energy for magnetization reversal of a single-4f-ionic single molecule magnet by a longitudinal contraction of the coordination space. *Inorg. Chem.* **2007**, 46, 7250.

5. Margheriti, L. Chiappe, D.; Mannini M.; Car, P.E.; Sainctavit, P.; Arrio, M.A.; Buatier de Mongeot, F.; Cezar, J.C.; Piras, F.M.; Magnani, A.; Otero, E.; Caneschi, A.; Sessoli, R. X-Ray Detected Magnetic Hysteresis of Thermally Evaporated Terbium Double-Decker Oriented Films. *Adv. Materials*, **2010**, 22, 5488.

6. Katoh, K.; Yoshida, Y.; Yamashita, M.; Miyasaka H.; Breedlove, B.K.; Kajiwara, T.; Takaishi, S.; Ishikawa, N.; Isshiki, H.; Zhang, Y.F.; Komeda, T.; Yamagishi, M.; Takeya, J.

Direct Observation of Lanthanide(III)-Phthalocyanine Molecules on Au(111) by Using Scanning Tunneling Microscopy and Scanning Tunneling Spectroscopy and Thin-Film Field-Effect Transistor Properties of Tb(III)- and Dy(III)-Phthalocyanine Molecules. *J. Am. Chem. Soc.* **2009**, 131, 9967.

7. Vitali, L.; Fabris, S.; Mosca Conte, A.; Brink, S.; Ruben, M.; Baroni, S.; Kern, K. Electronic Structure of Surface supported Bis(phthalocyonato) terbium (III) Single Molecular Magnets. *Nano Lett.* **2008**, 8, 3364.

8. Schwöbel, J.; Fu, Y.; Brede, J.; Dilullo, A.; Hoffmann, G.; Klyatskaya, S.; Ruben, M.; Wiesendanger, R. Real-space observation of spin-split molecular orbitals of adsorbed single-molecule magnets. *Nat. Commun.* **2012**, 3:953.

9. Fu, Y-S.; Schwöbel, J.; Hla, S.W.; Dilullo, A.; Hoffmann, G.; Klyatskaya, S.; Ruben, M.; Wiesendanger, R. Reversible Chiral Switching of Bis(phthalocyaninato) Terbium(III) on a Metal Surface. *Nano Letters*, **2012**, 12, 3931.

10. Ara, F.; Qi, Z.K.; Hou, J.; Komeda, T.; Katoha, K.; Yamashita, M. A scanning tunneling microscopy study of the electronic and spin states of bis(phthalocyaninato)terbium(III) ($TbPc_2$) molecules on Ag(111). *Dalton Trans.* **2016**, 45, 16644.

11. Komeda, T.; Isshiki, H.; Liu, J.; Zhang, Y.F.; Lorente, N.; Katoh, K.; Breedlove, B.K.; Yamashita, M. Observation of electric current control of a local spin in a single-molecule magnet. *Nat. Commun.* **2011**, 2, 217.

12. Komeda, T.; Isshiki, H.; Liu, J.; Katoh, K.; Yamashita, M. Variation of Kondo Temperature Induced by Molecule–Substrate Decoupling in Film Formation of Bis(phthalocyaninato) terbium(III) Molecules on Au(111), *ACS Nano*, **2014**, 8, 4866–4875.

13. Serrano, G.; Wiespointner-Baumgarthuber, S.; Tebi, S.; Klyatskaya, S.; Ruben, M.; Koch, R.; Mulleger, S. Bilayer of Terbium Double-Decker Single-Molecule Magnets, *J. Phys. Chem. C*, **2016**, 120, 13581–13586.

14. Malavolti, L.; Mannini, M.; Car, P.E.; Campo, G.; Pineider, F.; Sessoli, R. Erratic magnetic hysteresis of $TbPc_2$ molecular nanomagnets. *J. Mater. Chem. C*, **2013**, 1, 2935.

15. Mannini, M.; Bertani, F.; Tudisco, C.; Malavolti, L.; Poggini, L.; Misztal, K.; Menozzi, D.; Motta, A.; Otero, E.; Ohresser, P. et al. Magnetic behavior of $TbPc_2$ single-molecule magnets chemically grafted on silicon surfaces. *Nat. Commun.* 2014

16. Warner, B.; El Hallak, F.; Atodiresei, N.; Seibt, P.; Prüser, H.; Caciuc, V.; Waters, M.; Fisher, A.J.; Blügel, S.; van Slageren, J.; Hirjibehedin, S. Sub-molecular modulation of a 4f driven Kondo resonance by surface induced asymmetry. *Nat. Commun.* **2016**, 7:12785.

17. Ishikawa, N.; Sugita, M.; Wernsdorfer, W. Quantum tunneling of magnetization in lanthanide single-molecule magnets: bis(phthalocyaninato) terbium and bis(phthalocyaninato) dysprosium anions. *Angew. Chem. Int. Ed.* **2005**, 44, 2931.

18. Urdampilleta, M.; Klyatskaya, S.; Cleuzio, J.P.; Ruben, M.; Wernsdorfer, W. Supramolecular spin valves. *Nature Materials*, **2011**, 10, 502.

19. Vincent, R.; Klyatskaya, S.; Ruben, M.; Wernsdorfer, W.; Balestro, F. Electronic read-out of a single nuclear spin using a molecular spin transistor. *Nature*, **2012**, 488, 357.

20. M. Urdampilleta, Klyatskaya, S.; Ruben, M.; Wernsdorfer, W. Magnetic interaction between a radical spin and a single-molecule magnet in a spin valve. *ACS Nano*, **2015**, 9, 4458.

21. Müllegger, S.; Tebi, S.; Das, A.K.; Schöfberger, W.; Fachinger, F.; Koch, R. Radiofrequency scanning tunneling spectroscopy for single-molecule spin resonance. *Phys. Rev. Lett.* **2014**, 113, 133001.

22. Fahrendorf. S.; Atodiresei, N.; Besson, C.; Caciuc, V.; Matthes, F.; Blügel, S.; Kögerler, P; Bürgler, D.E.; Schneider, C.M. Accessing 4f-states in single-molecule spintronics. *Nat. Commun.* **2013**, 4:2425.

23. Katoh, K.; Komeda, T.; Yamashita, M. Surface morphologies, electronic structures, and Kondo effect of lanthanide(III)-phthalocyanine molecules on Au(111) by using STM, STS and FET properties for next generation devices. *Dalton Trans.*, **2010**, 39, 4708-4723

24. Gao, L.; Ji, W.; Hu, Y. B.; Cheng, Z. H.; Deng, Z. T.; Liu, Q.; Jiang, N.; Lin, X.; Guo, W.; Du, S.X.; Hofer, W. A.; Xie, X. C.; and Gao, H.-J. Site-Specific Kondo Effect at Ambient Temperatures in Iron-Based Molecules. *Phys. Rev. Lett.* **2007**, 99, 106402.

25. Zhao, A.; Li, Q.; Chen, L.; Xiang, H.; Wang, W.; Pan, S.; Wang, B.; Xia, X. Yang, J.; Hou, J.G.; Zhu, Q. Controlling the Kondo Effect of an Adsorbed Magnetic Ion Through Its Chemical Bonding. *Science*, **2005**, 309, 1542.

26. Fano, U. Effects of Configuration Interaction on Intensities and Phase Shifts. *Phys. Rev.* **1961**, 124, 1866.

27. Nagaoka, K.; Jamneala, T.; Gronis, M.; Crommie, M. Temperature dependence of a single Kondo impurity. *Phys.Rev. Lett.* **2002**, 88, 077205.

28. Mugarza, A.; Robles, R.; Krull, C.; Korytar, R.; Lorente, N.; Gambardella, P. Electronic and magnetic properties of molecule-metal interfaces: transition metal phthalocyanines adsorbed on Ag(100). *Phys. Rev. B* **2012**, 85, 155437.

29. Keziliebeke, S.; Amokrane, A.; Abel, M.; Bucher, J.P. Hierarchy of Chemical Bonding in the Synthesis of Fe-Phthalocyanine on Metal Surfaces: A Local Spectroscopy Approach. *J. Phys. Chem. Lett.* **2014**, 5, 3175.

30. Hla, S.W. Scanning tunneling microscopy single atom/molecule manipulation and its application to nanoscience and technology. *J. Vac. Sci. Technol.* B, **2005**, 23, 1351-1360.

31. Lu, X. ; Hipps, K.W. Wang, X.D. ; Mazur, U. Scanning Tunneling Microscopy of Metal Phthalocyanines: d^7 and d^9 Cases. *J. Am. Chem. Soc.* **1996**, 118, 7197.

32. Chizhov, I. ; Scholes, G. ; Kahn, A. The Influence of Steps on the Orientation of Copper Phthalocyanine Monolayers on Au(111). *Langmuir*, **2000**, 16, 4358.

33. Zhang, Q.; Kuang, G.; Pang, R.; Shi, X.; Lin, N. Switching molecular Kondo effect via supramolecular interaction. *ACS Nano*, 2015, 9, 12521-12528.

34. Kinoshita, M. An organic radical crystal showing spontaneous ferromagnetic order. In *pi-electron magnetism from molecules to magnetic materials*; Veciana, J., Ed.; Springer: Berlin, 2001; pp 1-32.

35. Yamaguchi, K. Electrons in specific molecular systems. In *From molecules to molecular systems;* Nagakura, S., Ed.; Springer: Tokyo, 1998; pp 67-91.

36. Repp, J. ; Meyer, G. ; Stojkovic, S.M. ; Gourdon, A. ; Joachim, C. Molecules on insulating films : Scanning tunneling microscopy imaging of individual molecular orbitals. *Phys. Rev. Lett.* **2005**, 94, 026803.

37. Villagomez, J.V. ; Zambelli, T. ; Gauthier, S. ; Gurdon, A. Berthes, C. ; Stojkovic, S. ; Joachim, C. A local view of hyperconjugation. *Chem. Phys. Lett.* **2007**, 450, 107-111.

38. Pavlicek, N. ; Mistry, A. ; Majzik, Z. ; Moll, N. ; Meyer, G. Fox, D.J. ; Gross, L. Synthesis and characterisation of triangulene. *Nature Nanotech.* **2017**, 12, 308 – 311.

39. Gillespie, R. J. Fifty years of the VSEPR model. *Coord. Chem. Rev.* **2008**, 252, 1315–1327.

40. Branzoli, F. ; Carretta, P. ; Filibian, M. ; Klyatskaya, S. ; Ruben, M. Low-energy spin dynamics in the $[YPc_2]^0$ S=1/2 antiferromagnetic chain. *Phys. Rev B.* **2011**, B83, 174419.

41. Paillaud, J.L. ; Drillon, M. ; De Cian, A. ; Fischer, J. ; Weiss, R. ; Villeneuve, G. Radical-based ferromagnetic chains in Yttrium Diphthalocyanine $[YPc_2]$ CH_2Cl_2. *Phys. Rev. Lett.* **1991**, 67, 244 – 247.

42. Hunter, C. A.; Sanders, J.K.M. The nature of pi-pi interaction. *J. Am. Chem. Soc.* **1990**, 112, 5525.

43. Kohn, W.; Sham, L. J. Self-Consistent Equations Including Exchange and Correlation Effects. *Phys. Rev.* **1965**, *140*, A1133-A1138.

44. CPMD; Copyright IBM Corp. 1990-2016, Copyright MPI für Festkörperforschung Stuttgart 1997-2001, http://www.cpmd.org/

45. Becke, A. D., Density-functional exchange-energy approximation with correct asymptotic behavior. *Phys. Rev. A* **1988**, *38*, 3098-3100.

46. Lee, C.; Yang, W.; Parr, R. G., Development of the Colle-Salvetti correlation-energy formula into a functional of the electron density. *Phys. Rev. B* **1988**, *37*, 785-789.

47. Stephens, P. J.; Devlin, F. J.; Chabalowski, C. F.; Frisch, M. J. *J. Phys. Chem.* **1994**, 98, 11623-11627

48. Troullier, N.; Martins, J. L. Efficient Pseudopotentials for Plane-Wave Calculations. *Phys. Rev. B* **1991**, *43*, 1993-2006.

49. Goedecker, S.; Teter, M.; Hutter, J. Separable Dual-Space Gaussian Pseudopotentials. Phys. Rev. B **1996**, *54*, 1703-1710.

50. Barnett, R.~N.; Landman, U. Born-Oppenheimer molecular-dynamics simulations of finite systems: Structure and dynamics of $(H_2O)_2$. *Phys. Rev. B* **1993**, *48*, 2081-2097.

51. Grimme, S. Semiempirical GGA-type density functional constructed with a long-range dispersion correction. *J. Comput. Chem.* **2006**, *27*, 1787-1799.

Graphical TOC Entry